# The cytoplasmic cage domain of the mechanosensitive channel MscS is a sensor of macromolecular crowding

lan Rowe, 1,2 Andriy Anishkin, 4 Kishore Kamaraju, 1 Kenjiro Yoshimura, 1,5 and Sergei Sukharev 1,3

Cells actively regulate the macromolecular excluded volume of the cytoplasm to maintain the reciprocal fraction of free aqueous solution that is optimal for intracellular processes. However, the mechanisms whereby cells sense this critical parameter remain unclear. The mechanosensitive channel of small conductance (MscS channel), which is the major regulator of turgor in bacteria, mediates efflux of small osmolytes in response to increased membrane tension. At moderate sustained tensions produced by a decrease in external osmolarity, MscS undergoes slow adaptive inactivation; however, it inactivates abruptly in the presence of cytoplasmic crowding agents. To understand the mechanism underlying this rapid inactivation, we combined extrapolated and equilibrium molecular dynamics simulations with electrophysiological analyses of MscS mutants to explore possible transitions of MscS and generated models of the resting and inactivated states. Our models suggest that the coupling of the gate formed by TM3 helices to the peripheral TM1-TM2 pairs depends on the axial position of the core TM3 barrel relative to the TM1-TM2 shaft and the state of the associated hollow cytoplasmic domain ("cage"). They also indicate that the tension-driven inactivation transition separates the gate from the peripheral helices and promotes kinks in TM3s at G113 and that this conformation is stabilized by association of the TM3b segment with the  $\beta$  domain of the cage. We found that mutations destabilizing the TM3b-β interactions preclude inactivation and make the channel insensitive to crowding agents and voltage; mutations that strengthen this association result in a stable closed state and silent inactivation. Steered simulations showed that pressure exerted on the cage bottom in the inactivated state reduces the volume of the cage in the cytoplasm and at the same time increases the footprint of the transmembrane domain in the membrane, implying coupled sensitivity to both membrane tension and crowding pressure. The cage, therefore, provides feedback on the increasing crowding that disengages the gate and prevents excessive draining and condensation of the cytoplasm. We discuss the structural mechanics of cells surrounded by an elastic cell wall where this MscS-specific feedback mechanism may be necessary.

### INTRODUCTION

Life, as we know it, is inseparable from water. Solvation sets chemical potentials for all soluble components inside and outside the cell, affects intermolecular interactions, drives hydrophobic assembly, and provides free space for diffusion and macromolecular dynamics (macro-MD). Crowding effects are strong because many equilibria and reaction rates inside the cell have generally steeper dependencies on the macromolecular excluded volume than on ionic strength or osmolarity by itself (Cayley et al., 1991; Minton, 1998; van den Berg et al., 1999; Ellis, 2001; Zhou et al., 2008). Although mutual compensatory mechanisms between increased ionic strength and macromolecular excluded volume exist, the primary purpose of osmoregulation is the maintenance of a sufficient amount of free water in the cytoplasm (Record

et al., 1998). Cells actively regulate their water content by accumulating or releasing ions and small compatible osmolytes (Wood, 1999), but the mechanisms that sense and define the setpoints for water activity and volume fraction are still unclear. Although several candidates for primary osmosensors in different organisms and cell types have been proposed (Reiser et al., 2003; Liedtke, 2005; Wood, 2007; Wang et al., 2012), no mechanistic hypothesis that would connect their function with the fractional volume of water exists.

Free-living microorganisms are frequently subjected to hydration stresses and possess robust osmoregulatory systems. In hyperosmotic conditions, bacteria accumulate ions and compatible organic osmolytes to retain water (Csonka and Hanson, 1991; Wood et al., 2001; Cayley

Downloaded from http://rupress.org/jgp/article-pdf/143/5/543/1793447/jgp\_201311114.pdf by guest on 02 December 2025

<sup>&</sup>lt;sup>1</sup>Department of Biology, <sup>2</sup>Department of Chemistry and Biochemistry, and <sup>3</sup>Maryland Biophysics Program, University of Maryland, College Park, MD 20742

<sup>&</sup>lt;sup>4</sup>Center for Computational Proteomics, The Huck Institutes of the Life Sciences, Pennsylvania State University, University Park, PA 16802

<sup>&</sup>lt;sup>5</sup>Department of Machinery and Control Systems, College of Systems Engineering and Science, Shibaura Institute of Technology, Minuma-ku, Saitama-shi, Saitama 337-8570, Japan

Correspondence to Sergei Sukharev: sukharev@umd.edu.

Abbreviations used in this paper: MD, molecular dynamics; MscS, mechanosensitive channel of small conductance; TM, transmembrane.

<sup>© 2014</sup> Rowe et al. This article is distributed under the terms of an Attribution–Noncommercial–Share Alike–No Mirror Sites license for the first six months after the publication date (see http://www.rupress.org/terms). After six months it is available under a Creative Commons License (Attribution–Noncommercial–Share Alike 3.0 Unported license, as described at http://creativecommons.org/licenses/by-nc-sa/3.0/).

and Record, 2003). Under steady growth conditions, the internal turgor (hydrostatic pressure) inside bacterial cells decreases with an increase in external osmolarity (Cayley et al., 2000). However, in the event of a sudden drop of external osmolarity, bacteria release accumulated osmolytes through several types of mechanosensitive channels acting as tension-activated release valves. Gradual increase of tension in the cytoplasmic membrane of Escherichia coli opens the low-threshold YbdG channel (Schumann et al., 2010), exhibiting an MscM-like activity, followed by the more conductive MscK (Li et al., 2002) and mechanosensitive channel of small conductance (MscS; Levina et al., 1999) and several other species such as YjeP, YbiO, and YnaI (Edwards et al., 2012). When tension in the membrane approaches the lytic limit (11-14 mN/m), large-conductance mechanosensitive channels (MscLs) release larger osmolytes (Sukharev et al., 1994) and rescue the cell from lysis (Levina et al., 1999). One should remember that in the event of moderate osmotic adjustments, even brief opening of the nonemergency MscS valve results in dissipation of vital ionic gradients and clearly comes at a metabolic cost. Apparently, to suppress spurious openings at sustained moderate tensions, MscS shows adaptive behavior that leads to closure and subsequent inactivation (Akitake et al., 2005, 2007; Boer et al., 2011; Kamaraju et al., 2011).

In the inactivated state, MscS does not conduct or respond to tension (Akitake et al., 2005). Examination of the WT MscS crystal structure (PDB ID 2OAU [Steinbacher et al., 2007]) obtained in foscholine (in the absence of lipids) suggests that its conformation resembles a nonconductive inactivated state (Sukharev et al., 2007). This state is characterized with the gate uncoupled from the external stimulus because of the splay of peripheral TM1-TM2 helical pairs being separated from the gate formed by sharply kinked TM3 helices. For the same reason, the structure does not possess functionally important D62–R131 bridges. A more recent crystal structure of WT MscS obtained in a partially open state in dodecylmaltoside (PDB ID 4HWA [Lai et al., 2013]) shows a different splay of unsupported TM1-TM2 pairs, indicating that the conformations of these domains are sensitive to the type of detergent replacing the membrane and that their positions in the lipid bilayer are likely to be different. Several attempts were made to create a model of the resting state, which would have a direct connection to transmit force from the lipid-facing helices to the gate (Akitake et al., 2007; Anishkin et al., 2008a; Vásquez et al., 2008; Belyy et al., 2010a). This conformation is likely characterized by a more parallel packing of TM1-TM2 helices, forming a buried hydrophobic interface with TM3s (see Fig. 1), from where the channel would be able to open by membrane tension transmitted through the peripheral helices to its gate (Belyy et al., 2010a). The previous searches for the gating-competent resting state and

models for opening and inactivation considered primarily conformational changes in the transmembrane (TM) domain, although there were indications that the movements of the TM domain generates coupled movements in the "cage" (Koprowski et al., 2007; Nomura et al., 2008; Machiyama et al., 2009).

The possibility of a salt bridge formation between the tips of the TM1-TM2 loops (D62) and the equatorial region of the cage (R128/R131) was first noted in MD simulations (Sotomayor and Schulten, 2004), and the functional role of these bridges was experimentally demonstrated by Nomura et al. (2008), who found that disruption of these bridges with mutations strongly speeds up channel adaptation. Another important observation was made by Grajkowski et al. (2005), who first reported that adaptive closure of MscS comes much faster in the presence of indifferent polymers such as polyethylene glycols, dextrans, or Ficoll on the cytoplasmic side, implying involvement of the hollow cage domain. Subsequent genetic screens for gain- and loss-of-function mutants performed by the same group (Koprowski et al., 2011) revealed multiple new loci affecting gating, including one potent mutation at the interface between TM3b and the  $\beta$  domain of the cage (G168D) that strongly affected the process of adaptation.

In the present paper we go beyond previous studies and show that MscS inactivation is exquisitely sensitive to excluded volume effects and that the cage domain directly participates in sensing the cytoplasmic crowding of large-molecular-weight compounds and voltage. We develop a new molecular model of the resting state that includes several previously unaccounted features and propose a consistent explanation for the role of the cage and specifically the TM3b-β interface in the functional cycle of MscS. We show opposite effects of interface-stabilizing and destabilizing mutations on MscS inactivation, suggesting that in active states the mutual arrangement of TM3b and β domains are likely to be different from that in the crystal structure. Molecular simulations of the resting and inactivated state models illustrate how geometrical parameters of the molecule (lateral expansion of the TM domain and compaction of the cytoplasmic cage) lead to the coupling between membrane tension and crowding pressure, both acting synergistically in driving the inactivation transition. We propose the first structural mechanism of crowding sensing by a mechanosensitive channel and discuss the physiological context in cells surrounded by elastic peptidoglycan, where this function might be particularly important.

### MATERIALS AND METHODS

### Modeling and simulations

We used the extrapolated motion protocol (Akitake et al., 2007; Anishkin et al., 2008b) to generate a set of nonrandom models from the crystal structure of WT MscS (PDB ID 2OAU [Steinbacher et al., 2007]). The unresolved N-terminal domain was modeled with Rosetta (Anishkin et al., 2008a). Arranged as cycles of small (0.1–0.5 Å) displacements extrapolated from the previous step, energy minimizations, and short relaxing MD simulations (see details in the supplemental text), this protocol generates strings of interconnected conformations covering 5–15-Å domain displacements within 50-100 steps. The protocol was implemented with the Tcl/ Tk language in NAMD2-VMD (Humphrey et al., 1996). The library of ~86,000 models generated from different starting points was sorted using automated searching scripts identifying spatial proximities of specific groups or domains. The specific search criteria included (a) sufficiently tight rings of L105 and L109 forming a nonconductive gate, (b) intersubunit salt bridge between the tip of the TM1-TM2 loop (D62) and the equatorial region of the cytoplasmic cage domain (R128 or R131; Nomura et al., 2008), (c) an extensive buried contact between TM2 (A63-F80) and TM3 (V99-L115) in the resting state and separation of these helices in the inactivated state (Belyy et al., 2010a), and (d) TM3 helix straightened near G113 in the resting state or kinked in the inactivated state (Akitake et al., 2007). An additional criterion for the choice of the pair of resting and inactivated states was the difference of the effective in-plane areas of the TM barrel that was estimated from the inactivation and recovery kinetics as  $\sim$ 8 nm<sup>2</sup> (Kamaraju et al., 2011).

The candidate models without perturbations of the secondary structure were embedded in the fully hydrated and preequilibrated lipid bilayer assembled from 220 POPC molecules, energy minimized, and then equilibrated in all-atom MD simulations for 20 ns, followed by refinement using a 5-ns symmetry-driven simulated annealing (Anishkin et al., 2010).

To explore the structural changes in MscS under increased crowding in the cytoplasm, we visualized the effect of cytoplasmic cage compression using steered MD. We have approximated the pressure of the large macromolecules by a force acting on the C-terminal half of the cytoplasmic cage (residues 183–280 in each subunit, 2,751 atoms per complex). The force acting toward the midplane of the bilayer was set for slow exponential growth from 0.001 to 0.1 kcal/mol/Å/atom over the course of 20-ns simulations. To prevent the net displacement of the protein and membrane under the force, we have restrained the center of mass of nonhydrogen backbone atoms of TM1–TM2 helices in its position inside the lipid bilayer only in the direction normal to the membrane midplane (see more details in the supplemental text).

### Mutagenesis and electrophysiology

The *mscS* gene was housed in the IPTG-inducible pB10b vector and expressed in the MJF465 triple-knockout *E. coli* strain (*mscS*<sup>-</sup>, *mscL*<sup>-</sup>, *mscK*<sup>-</sup>; Levina et al., 1999) or PB113 (*mscS*<sup>-</sup>, *mscK*<sup>-</sup>; Li et al., 2002), which retained a native copy of *mscL*. Mutants of MscS were created using a QuikChange mutagenesis kit (Agilent Technologies).

Spheroplasts were generated as described in previous works (Martinac et al., 1987; Yoshimura et al., 2001; Akitake et al., 2005), and all recordings were made in excised inside-out patches exposing the cytoplasmic side to the bath. The experimental bath solution contained 400 mM sucrose, 200 mM KCl, 50 mM MgCl<sub>2</sub>, 5 mM CaCl<sub>2</sub>, and 5 mM HEPES and was titrated to pH 7.4 with KOH. For crowding experiments, Ficoll 400 was perfused into the bath manually at the desired wt/vol concentration. Osmolarities of solutions were measured with a Wescor 5520 vapor pressure osmometer. Membrane patches were obtained with borosilicate glass pipettes (Drummond) and recorded by an Axopatch 200B amplifier (Molecular Devices); unless otherwise noted, all recordings were performed at 30 mV (pipette potential). Negative pressure (suction) was applied using a high-speed pressure clamp apparatus (HSPC-1; ALA Scientific). Pressure and voltage protocol programming and data acquisition/analysis were performed with the PClamp 10 suite (Axon Instruments). Linear triangular ramps were used to determine activation midpoints and hysteresis, pulse-step protocols elucidated the closing rate dependencies on tension, and pulse-step-pulse protocols gave insight to the extent of tension-driven inactivation.

Conversion of the pressure amplitudes into the tension scale was achieved by using the previously established midpoint tensions for WT MscS ( $\gamma_{0.5}$  = 7.8 mN/m) and MscL ( $\gamma_{0.5}$  = 13 mN/m) with the ratio of 0.6 (Belyy et al., 2010b). Assuming that the radius of curvature of the patch (r) does not change in this pressure range, according to the Young-Laplace law ( $\gamma$  = pr/2) the ratio of tension and pressure midpoints should be the same. MscS mutants with unknown midpoints were expressed in the PB113 strain carrying WT MscL. Patches were probed with linear pressure ramps, and the activation pressure midpoints for MscS and MscL were determined. From the ratio of pressure midpoints and  $\gamma_{0.5}$  for MscL, we calculated  $\gamma_{0.5}$  for MscS.

### Online supplemental material

The supplement text contains technical details of MD simulations. Fig. S1 shows a magnified view of the side chain packing at the TM3b– $\beta$  domain interface. Figs. S2 and S3 show a scheme illustrating the functional cycle of MscS and its alteration in interface-stabilizing mutants, respectively. Figs. S4 and S5 show the effect of polyethylene glycol on MscS inactivation, which parallels the effect of Ficoll and the effect of smaller osmolyte trehalose, respectively. Table S1 summarizes gating phenotypes for several mutants with altered contact region between the C-terminal segment (TM3b) of the gate-forming TM3 helix and the  $\beta$  domain of the MscS cage. Online supplemental material is available at http://www.jgp.org/cgi/content/full/jgp.201311114/DC1.

### RESULTS

### Modeling

The existing crystal structures of E. coli MscS (Steinbacher et al., 2007; Wang et al., 2008; Lai et al., 2013) and its homologues (Zhang et al., 2012) solved in detergents obviously do not represent the complex functional cycle of the channel entirely. The nonconductive structures likely resemble the inactivated state with an uncoupled gate (Steinbacher et al., 2007), whereas conductive conformations (Wang et al., 2008; Lai et al., 2013) appear to be partially open. Modeling and simulations may help envision the channel structure in the native membrane environment and reconstruct the missing parts of the functional cycle (Akitake et al., 2007; Anishkin et al., 2008a,b). Here we combined a computational algorithm allowing us to explore the conformational space of MscS with multiple constraints derived from functional experiments to generate models for the resting and inactivated states.

A database of nonrandom models was generated from the revised crystal structure of WT MscS. This library of 86,000 nonrandom models was sorted using automated searching scripts identifying spatial proximities of specific groups or domains. The criteria included a nonconductive gate, salt bridge formed between D62 and one of the arginines (R128 or R131) on the cytoplasmic cage domain, buried contact between TM2 and TM3 engaging the gate in the resting state, or separation of these helices in the inactivated state.

It soon became obvious that imposition of the D62–R131 bridges results in a more upright orientation of the peripheral helices and vertical displacement of the TM3 barrel inside the TM1–TM2 shaft. In extrapolated motion protocol trials, this transformation generally (not always) correlated with straightening of the crystallographic G113 kink and reformation of a less prominent kink near G121. In the crystal-like inactivated state, D62 formed a salt bridge with R128. We did not stipulate the in-plane area change in the TM domain between the modeled resting and inactivated states, but we found it very close to the experimentally estimated 8 nm² (Kamaraju et al., 2011).

The candidate models were embedded in the fully hydrated and preequilibrated POPC lipid bilayer, energy minimized, and equilibrated in all-atom MD simulations for 20 ns, followed by symmetry-driven simulated annealing (Anishkin et al., 2010). The models are shown in Fig. 1 (A and B), with the detailed structure of the gate region and surrounding domains shown in Fig. 1 (C and D).

The conformation assigned as inactivated (Fig. 1 A) is similar to the initial crystal state, with prominent kinks at G113 and tight packing of the TM3b– $\beta$  interface.

In this putative inactivated conformation, the peripheral TM1/TM2 helices are splayed but at a smaller angle than in the crystal structure, allowing the D62-R128 salt bridges to form. The TM1-TM2 pairs are partially detached from the gate region such that the hydrophobic side chains in the buried zone are packed more loosely than in the resting state. The TM1-TM2 splay increases the effective in-plane area of the lipid-embedded TM domain compared with the resting state (Fig. 1 B). In most of the candidate models for the resting conformation, the TM3 helices were reproducibly kink-free until G121, the entire TM3 barrel was moved up inside the sheath of peripheral TM1-TM2 helices, and the TM3b helical segments were dissociated from the  $\beta$  domains within the cytoplasmic cage. The changes in side chain packing associated with the detachment of TM3b's from β domains are shown in Fig. S1.

The transition from left to right would represent recovery from inactivation to the gating-competent resting state. Experimental measurements of recovery kinetics show that it is a relatively slow process in molecular scale taking, 1.3–2 s for WT MscS (Akitake et al., 2005). It involves several changes: compact packing of helices

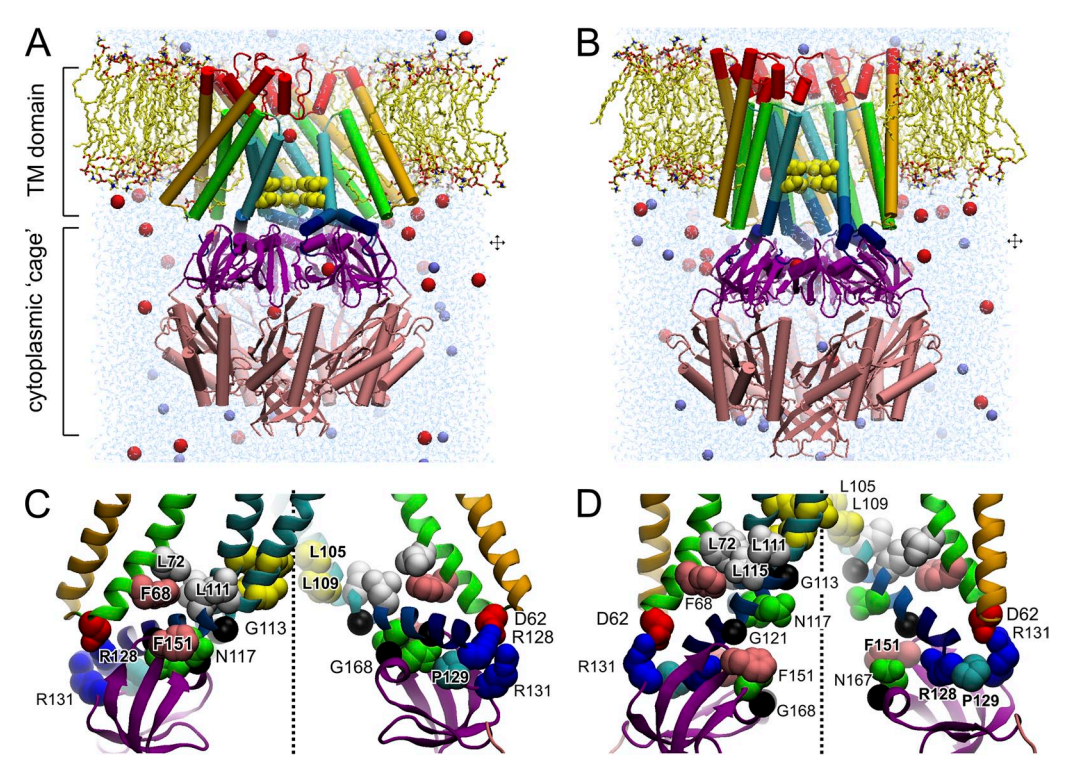


Figure 1. Modeling of the resting and inactivated states of MscS based on the crystal structure predicts simultaneous changes at the TM2–TM3 and TM3b– $\beta$  domain interfaces. (A and B) Displayed are MD-equilibrated models of the inactivated (A) and resting (B) states in the explicit lipid bilayer. (C and D) The details of TM cage domain interactions with critical side chains shown for the inactivated (C) and resting (D) state where the gate (L105 and L109) is coupled to the peripheral helices through the hydrophobic TM2–TM3 (F68, L72–L111, and L115) contact. The model of the inactivated state resembles the crystal conformation (PDB ID 2OAU); however, the splay of the peripheral TM1 and TM2 helices (ocher and green) is less. In both conformations, D62 residing on the TM1–TM2 loop forms a salt bridge with either R128 in the inactivated or R131 in the resting state. The resting state model predicts straightening of the crystallographic G113 kink, a substantial separation of TM3b (dark blue) from the  $\beta$  cytoplasmic domain (purple), and a translation of the gate region upward.

and formation of a more extended and tight contact between TM2 and TM3 (Fig. 1, C and D), which are accompanied by movement of the TM3 barrel inside the TM1-TM2 sheath by approximately two helical turns (from the cytoplasmic interface toward midplane of the membrane), straightening of TM3s, and detachment of the TM3b helical segment from  $\beta$  domains and reformation of D62-R131 bridges, which stabilize the resting state. The inactivating transition is likely to involve the same changes in reverse, which results in a visible decrease of the cage profile in the cytoplasm. Although its own internal volume does not change much, because of the vertical displacement, the cage occupies a smaller volume when the sharp kinks at G113 are in place and the TM1-TM2 pairs are separated from the inner TM3 barrel.

We have also identified an intermediate conformation in which the TM3b segments are partially attached to the  $\beta$  domains, but the peripheral TM1–TM2 pairs are in the upright position, attached to the gate, and form the salt bridges with the cage. This conformation may take place in N117V and N167V mutants described below (see also Figs. S2 and S3).

# MscS inactivation is increased in the presence of crowding agents

Like activation, MscS inactivation is driven by tension; both transitions originate from the closed state (Kamaraju et al., 2011). The ability of MscS current to adapt with time under sustained tension (Akitake et al., 2005; Belyy et al., 2010b) produces decaying current traces that represent the sum of sequential processes of adaptive closure and complete inactivation. The two kinetically intertwined processes are distinguished by the "comb" pressure protocol that includes a prolonged conditioning step of tension with interspersed short saturating pulses testing for the availability of noninactivated channels. In control experiments, the amplitude of current responses to test pulses gradually decays with time, representing the kinetics of tension-dependent inactivation (Fig. 2).

The presence of crowding agents such as Ficoll 400 on the cytoplasmic side shifts the activation curve in response to ramp stimuli toward higher pipette pressures (Fig. 3 A), signifying that the crowding pressure acting primarily on the cytoplasmic domain interacts with the gate and counteracts the tension. The presence of crowders also changes the character of response to the comb protocol (Fig. 2), leading to immediate inactivation after the first test pulse. In the presence of 10% Ficoll, the rate of inactivation increases by more than one order of magnitude, as measured at the same amplitude of conditioning pulse equal to the midpoint pressure (p0.5) of MscS activation determined in ramp experiments. Surprisingly, the presence of 10% Ficoll did not visibly change the kinetics of recovery (Fig. 2 B).

Polyethylene glycol (PEG 3350) at a concentration of 25 mM ( $\sim$ 7.5 vol%) exerted the same strong effect on inactivation and slowed down the recovery (Fig. S4).

### The TM3b- $\beta$ domain interface

To proceed with analysis of mutations, we first visualized (Fig. 1 and Fig. S1) and analyzed the residue interactions at the TM3-β domain interface, which underwent a substantial rearrangement upon modeled transition from the inactivated to resting state. In the TM3b-βbound conformation representing the crystal-like inactivated state (Fig. S1 A), we observe several critical interactions. The side chain of N117 interacts with the backbone nitrogen of N167 and packs with F151. The backbone of N117 forms α-helical hydrogen bonds with the backbone of both critical hinge residues, G113 and G121 (Akitake et al., 2007). Besides the terminal oxygen of N117, the backbone of N167 also interacts with the backbone amide oxygen of F151. G168 packs in close proximity of G113 and N117. The crystallographic TM3–β contact is predicted to be essentially desolvated.

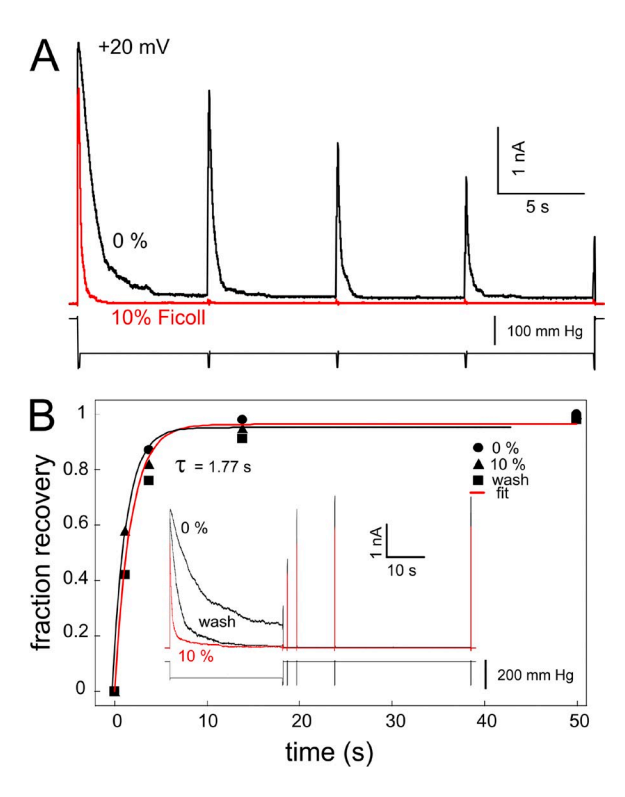


Figure 2. Responses of WT MscS to crowding agent Ficoll 400. (A) The trace was recorded at 20-mV pipette voltage with stimulation by a 30-s step of constant pressure with five evenly interspersed saturating test pulses of 0.1 s in length (comb protocol). The peaks of current responses to test pulses in the control (0% Ficoll 400) reflect the kinetics of inactivation. In the presence of 10% Ficoll, the MscS population opens in response to the first pulse and then completely inactivates. (B) The kinetics of recovery after inactivation. The inset shows the pressure protocol consisting of a prolonged step of pressure followed by a series of test pulses. The kinetics of recovery is not influenced by 10% Ficoll.

Upon straightening of TM3 in the resting state (Fig. S1 B), the hydrophobic neighborhood is largely dispersed, liberating the side chains of N117 and N167. The separation of many hydrophobic side chains is energetically feasible because N167 and N117 become favorably solvated. The general prediction is that crystallographic packing will be stabilized by isovolumic replacement of N117 or N167 by apolar valines. The G168D mutation identified by Koprowski et al. (2011) in the random mutagenesis screen is located at the interface between the cytoplasmic β domain and the C-terminal end of TM3b. Introduction of a charged and bulkier substitution is expected to stabilize the open conformation, which has the most unfolded TM3b-β contact. We have analyzed 10 single and 3 double substitutions in this region, as summarized in Table S1. The most drastic and interpretable effects of several mutations are described below.

### The G168D mutation affects the gating transitions and sensitivity to crowding agents

Current responses to triangular ramps of pressure for WT and G168D MscS are presented in Fig. 3 A. WT exhibits moderate asymmetry of response (hysteresis), showing a lower midpoint of the current-pressure curve on the descending limb of the ramp in comparison with the ascending limb, whereas G168D exhibits much stronger hysteresis and closes only at tensions near zero. The hysteresis is the manifestation of a slow closing rate  $(k_{off})$ , which appears to be especially slow in the mutant. This closing transition was confirmed with a specific (pulse-step) protocol; the population was subjected to a full activation by a short saturating pulse followed by a prolonged step of lower pressure, during which the closing kinetics were recorded. The resultant decaying current traces (Fig. 3, B and C) were fitted with monoexponential functions, producing a linear dependency

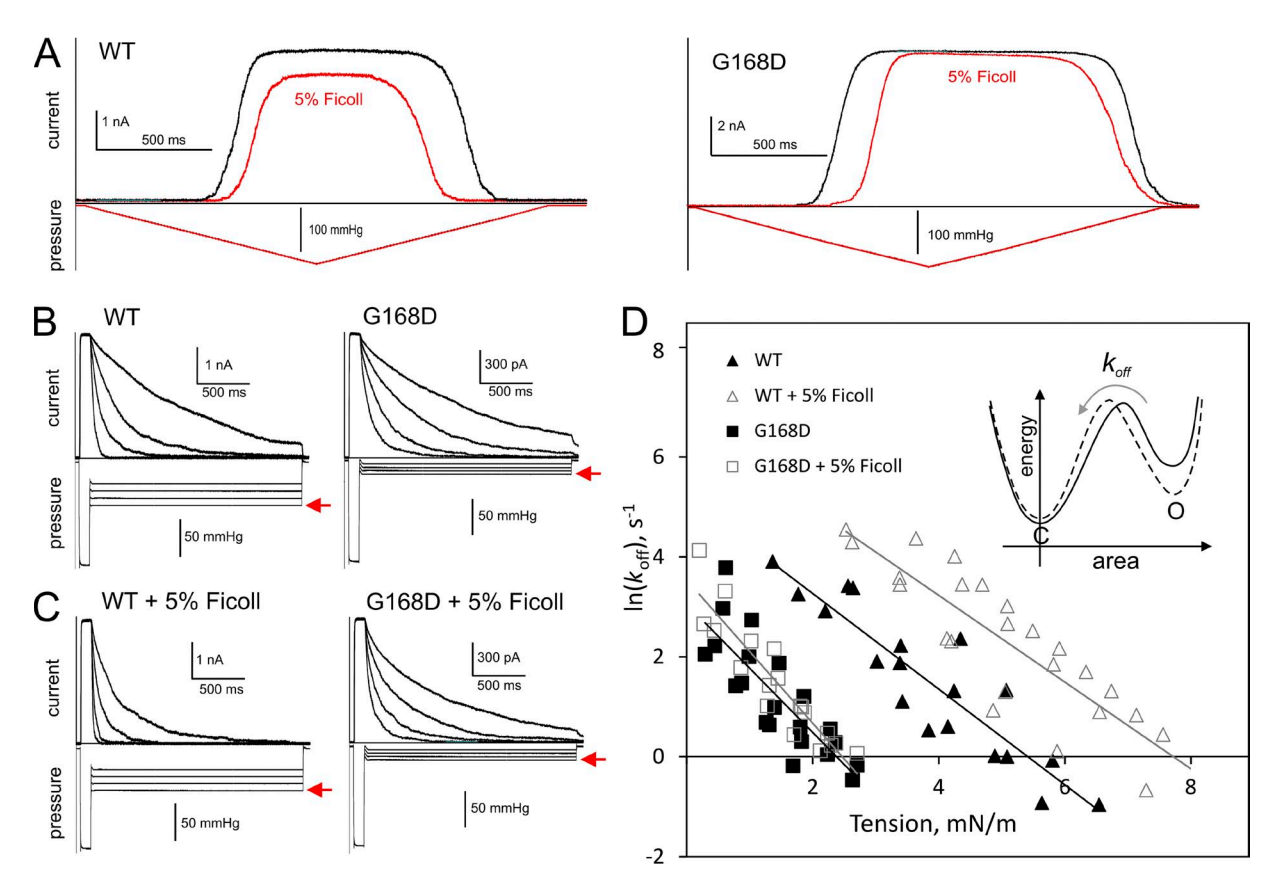


Figure 3. The crowding effects of 5% Ficoll 400 on WT and G168D MscS opening and closing. (A) Under symmetric ramps of saturating pressure, both WT and G168D MscS open at similar tensions yet G168D closes much more slowly, resulting in greater hysteresis of the closing portion of the activation curve. Upon the addition of 5% Ficoll, activation curves for both WT and G168D shift  $\sim$ 10% to the right (shown in red). (B and C) Pulse-step protocols revealing the kinetics of channel closure ( $k_{off}$ ) at different tensions for both WT and G168D. The current relaxation traces are shown before (B) and after (C) the addition of 5% Ficoll. Arrows indicate the pressure that was applied for the 2-s step during which the closing kinetics were monitored. (D) The closing rates from each of these curves (before and after 5% Ficoll) are plotted against the applied tension (n = 3 for each). The alteration of closing kinetics after 5% Ficoll is more pronounced for WT than G168D MscS. The inset shows a theoretical single barrier energy profile. The solid line represents the transition from closed to open in WT MscS, whereas the dashed line corresponds to G168D; the deeper and wider energy well for the open state of the mutant indicates a stabilization of the open state and a slower closing rate.

of the natural log of  $k_{off}$  on tension ( $\gamma$ , mN/m; Fig. 3 D). The same range of decay times was achieved for the G168D mutant at much lower pressures (Fig. 3, B and C, red arrows), which shifts the position of the  $ln(k_{off})$  curve to much lower tensions (by 2 mN/m). Extrapolation of the fitting line to zero tension (the y intercept) gives estimations of intrinsic closing rates of 2,430  $\pm$  270 s<sup>-1</sup> (n = 6) for WT and only  $107 \pm 24 \text{ s}^{-1}$  (n = 6) for G168D MscS. The slopes of these curves represent the tension dependency of their closing rates and can be interpreted as the difference of in-plane areas between the open state and rate-limiting barrier for closing, based on a putative single-barrier energy profile (Fig. 3 D, inset) for the tension-gated transitions (Sukharev et al., 1999). The slope of the WT curve was found to be  $-1.54 \pm$  $0.16 \text{ s}^{-1}/(\text{mN/m})$  (n = 6), which is smaller than that found for the G168D mutant  $(-2.0 \pm 0.17 \text{ s}^{-1}/(\text{mN/m});$ n = 6). This suggests that the open state of G168D is more stable and might have a deeper and/or wider energy well than WT. Equivalently, the mutant may have a different position of the rate-limiting barrier, which is farther from the bottom of the open-state well compared with WT.

Ramp responses measured in the presence of 5% wt/vol Ficoll 400 showed a  $10 \pm 6\%$  (n = 10) shift of the activation curve midpoint toward higher pressures for WT MscS, as measured on the ascending limb of the ramp (Fig. 4 A, red trace). The midpoint on the descending limb also shifted toward higher pressures ( $22\% \pm 10\%$ , n = 10), signifying stabilization of the resting state compared with the open state. The maximal current amplitude

at saturating tensions also tended to decrease by 10–20% as the result of partial inactivation of the channel population. For the G168D mutant, the response to the ascending limb shifted comparably with the WT; however, the rate of channel closure did not appear to increase as dramatically as in WT, and a decrease of maximal current was less pronounced. The alteration of closing rates by Ficoll was further investigated by repeating the pulse-step protocol for WT and the mutant (Fig. 3 C). The closing rate versus tension plot, based on three separate patches of both WT and G168D in the presence of 5% Ficoll, shows that the WT MscS curve shifts by  $\sim 40\%$  toward higher tension, whereas the G168D curve only has a 4% shift (Fig. 3 D, gray lines). This indicates that the G168D mutant is less susceptible to crowder-induced alterations of the closing rate of the channel.

Fig. 4 shows the typical responses of WT and G168D MscS to pulse-step-pulse protocols, revealing the degree of tension-dependent inactivation. After a 10-s conditioning step of approximately half the tension required to open all the channels (p0.5), a mean of  $\sim$ 70% of the WT population remained active, whereas the remaining channels recovered from inactivation with a time constant  $\tau$  of 1.4 + 0.4 s (n = 10). However, in the presence of 10% Ficoll, WT MscS inactivated completely, as demonstrated in Fig. 4 A. The G168D population generally resisted inactivation under similar conditions (10-s conditioning step of subsaturating tension), even in the presence of Ficoll (Fig. 4 B). To compare the inactivation resistance of G168D with another noninactivating mutant, G113A, we applied the same protocol.

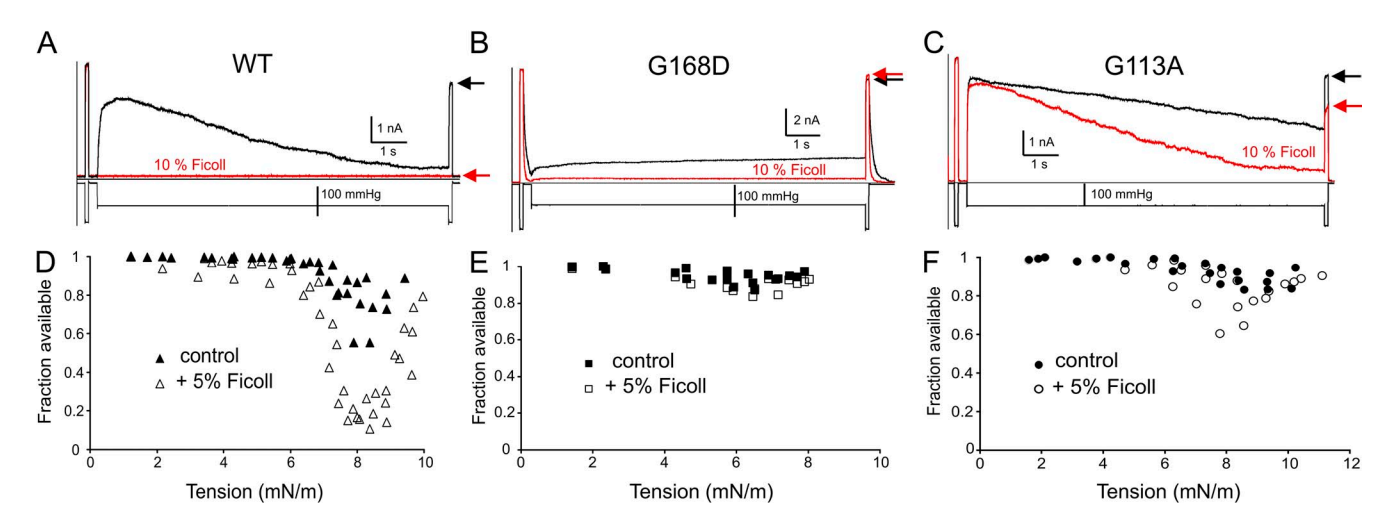


Figure 4. The crowding effect of Ficoll 400 on WT, G168D, and G113A MscS inactivation. (A–C) Pulse-step-pulse protocols were used to investigate the tension-driven inactivation of WT (A), G168D (B), and G113A MscS (C), with the difference between the initial and final pulse (black arrows) representing the relative amount of inactivation. After exposure to 10% Ficoll on the cytoplasmic side of the patch, WT MscS completely inactivates, G168D resists inactivation, and G113A displays an intermediate amount of inactivation (red arrows). (D–F) The same pulse-step-pulse protocol was applied at varying step pressures to several different patches of WT, G168D, and G113A (n=3 for each) in the absence and presence of 5% Ficoll 400. The resulting fraction of available channels was plotted against tension to illustrate inactivation. The inactivation of WT MscS channels was greatly increased in the presence of Ficoll (D), whereas G168D remained largely unchanged (E) and G133A inactivated moderately (F). In the experiments requiring multiple stimulations (D–F), we used a lower concentration (5%) of Ficoll because 10% severely compromises the stability of patches.

The G113A mutation favors a straight pore-lining helix and has been shown to impede inactivation in the absence of crowders (Fig. 4 C; Akitake et al., 2007; Kamaraju et al., 2011). Upon the addition of 10% Ficoll, G113A showed moderate inactivation. Fig. 4 D shows data from three WT MscS patches and describes the inactivation of the channels in response to 10-s conditioning steps of varying tension. WT MscS shows its maximal inactivation of roughly 40-50% of channels upon exposure to a 10-s step of tension of  $\sim 8$  mN/m, seen as a dip in the data. Upon addition of 5% Ficoll, this inactivation drastically increases, with 80-90% of the population becoming inactivated. G168D is much less susceptible to tensiondriven inactivation in identical procedures, with <15% inactivation (Fig. 4 E). After exposure to 5% Ficoll, inactivation remains <20% for G168D (n = 3). G113A shows intermediate inactivation ( $\sim$ 40%, n=3) in the presence of Ficoll, as seen in Fig. 4 F, indicating that the mutant is more sensitive to crowding than G168D. The fact that G168D inactivates much less than G113A in the presence of crowders indicates that the intact TM3b-β interface has a stronger contribution in the stability of the inactivated state than helical flexibility at G113 and that the cage is intimately involved in conveying the crowding pressure perturbation to the gate. Notably, the active channel population is entirely present in the first saturating test pulses in the 10-s protocol for both WT, G168D, and G113A (Fig. 4, A-C); this shows that crowding agents at these concentrations do not drive

the channel directly into the inactivated state and tension is absolutely required to inactivate MscS.

We have also tested the disaccharide trehalose, a compatible osmolyte, for similar effects in a concentration range up to 1 M, which constitutes 24 vol%. Although at this concentration trehalose also shifted activation curves to the right, it did not change the extent of inactivation of WT or G168D MscS (Fig. S5).

### G168D MscS is insensitive to voltage

Fig. 5 shows traces of MscS currents evoked by the same step-pulse pressure protocol recorded at different voltages.

The near-saturating step kept the entire population open for 5 s, whereas the super-saturating step at the end was applied to indicate any adaptive closure or inactivation that could occur during the step. As seen from the traces, the WT population reduced its conductance at -60 mV pipette voltage (depolarizing) and quickly closed and completely inactivated at -80 and -100 mV, consistent with the previous results (Akitake et al., 2005). An alanine substitution at residue 168 did not change this behavior. The G168E mutant displayed slight inactivation at -100 mV, and the G168D mutant showed no inactivation at all. These data suggest that the conformational changes in the cage are also critical for voltage-dependent inactivation, which likely proceeds through the common pathway with tension-dependent inactivation involving kink-stabilizing TM3b-β interactions. Based on a recent study (Cox et al., 2013), it is also possible that the cage

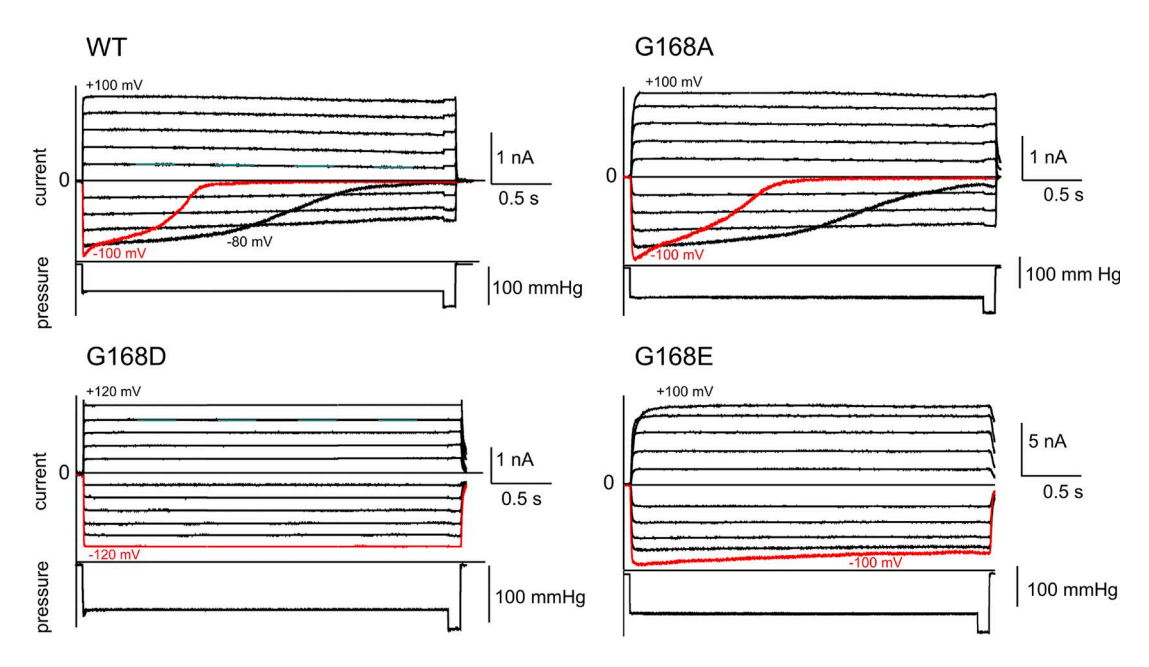


Figure 5. Adaptation and inactivation of MscS under strong depolarizing voltages is obliterated by negatively charged substitutions for G168. Responses of a 3-s step-pulse pressure protocol activate the entire population of channels in an excised membrane patch. This protocol was repeated at varying voltages between ±20 mV and ±120 mV to demonstrate the voltage-dependent adaptation and inactivation of WT MscS at -80 and -100 mV. A substitution of alanine at residue 168 does not cause a phenotypic divergence from WT MscS in terms of voltage-dependent adaptation. However, this voltage sensitivity is completely lost in G168D, whereas G168E shows little adaptation.

acts indirectly as a voltage sensor, in contrast to previous conjectures that charges on TM1 may be responsible for voltage-dependent gating (Bass et al., 2002). It is likely that the driving force for closure is electroosmotic water flux (Anishkin et al., 2008b), which may lead to partial desolvation and shrinkage of the cage, which would be analogous to the desolvating effect of crowders.

## Hydrophobic substitutions near the TM3b- $\!\beta$ interface stabilize nonconductive states

As suggested by the comparison of the inactivated and resting conformations (Fig. 1 and Fig. S1), disruption of the hydrophobic neighborhood of residues forming the TM3b– $\beta$  domain interface is facilitated by the presence of two polar residues, N117 and N167. Isovolumic replacement of these asparagines with more hydrophobic valines is predicted to stabilize the tightly assembled crystallographic state.

Fig. 6 compares the traces of N117V and N167V MscS populations versus WT obtained with ramp, pulse-step, and pulse-step-pulse protocols. WT showed full activation with 1-s ramps, its closure within a 10-s period took place at tensions near the midpoint, and it moderately

inactivated during a 5-s step and recovered with a characteristic  $\tau$  of 1.4  $\pm$  0.4 s (n = 10; see also Table S1). In the presence of a high concentration of crowders (10–15%), ramp responses showed only partial activation of MscS, whereas the rest of the population inactivated silently without opening (red trace). As indicated by measurements in the PB113 mscL-positive strain, both valine mutants activated at much higher tension than WT ( $\sim$ 13 mN/m). N117V showed reduced activation with a 1-s ramp and closed with a  $\tau$  of  $\sim$ 0.1 s at tensions close to 90% of saturating tension. This indicates substantial silent inactivation and a destabilized open state in this mutant. Under a 5-s conditioning step of subsaturating tension, N117V closed very quickly and inactivated almost completely. However, this mutant recovered three times faster than WT, with a  $\tau$  of 0.5  $\pm$  0.02 s (n = 3). N167V could not be readily activated by a 1-s ramp, also indicating massive silent inactivation preceding opening. It was impossible to keep this mutant population in the open state for longer than 500 ms, even under saturating pressure, indicating a strongly destabilized open state. Under pulse-step-pulse protocols, N167V inactivated silently and completely yet also recovered much

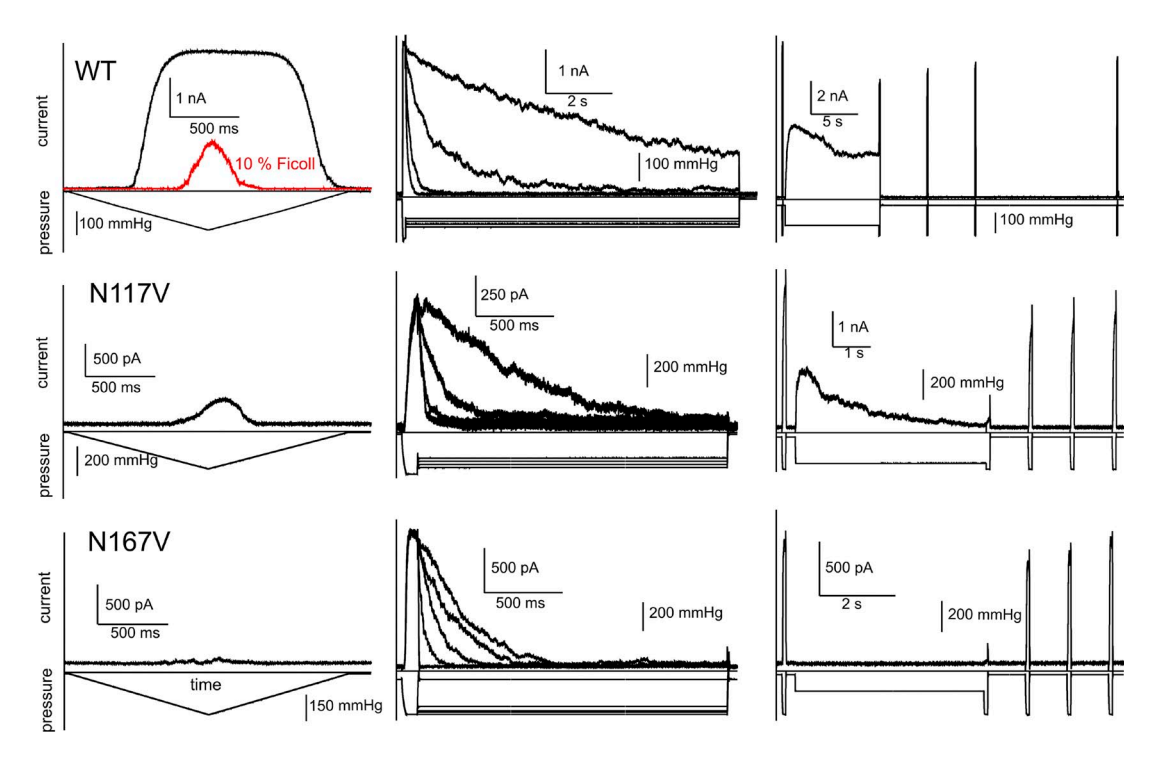


Figure 6. Effects of hydrophobic substitutions for N117 and N167 on the resting, open, and inactivated states. Three similar protocols for WT MscS and the mutants N117V and N167V are shown. (left) Upon being subjected to a 1-s pressure ramp, WT MscS displays its characteristic opening and closure, whereas both N117V and N167V refuse to open. (middle) The patches were then subjected to a closure protocol similar to those from Fig. 4 (B and C). N117V and N167V require near-saturating pressure to hold the channels open long enough to monitor closure, and both close much faster than WT MscS. (right) Lastly, the patches were subjected to an inactivation protocol beginning with a saturating pulse followed by a conditioning step and ending with several pulses of saturating pressure to monitor the process of channel recovery from the inactivated state. The N117V and N167V MscS mutants showed more inactivation than WT MscS after the conditioning step, yet both mutants recovered faster, with a characteristic time of recovery ( $\tau$ ) of 0.5  $\pm$  0.02 s (n = 3) for N117V and 0.6  $\pm$  0.2 s (n = 3) for N167V. Both of these recovery rate values were lower than that found for WT MscS (1.4  $\pm$  0.4 s; n = 10).

more quickly than WT MscS, with a  $\tau$  of  $0.6 \pm 0.2$  s (n = 3). When these two valine mutations were combined to create N117V/N167V MscS, the channel was again nearly impossible to activate with a 1-s ramp and showed complete inactivation under moderate tension (not depicted).

Silent inactivation from the resting state and quick recovery suggests that in these mutants the resting state is conformationally closer to the inactivated state. It appears that these transitions occur without substantial separation of TM3b from the  $\beta$  domain and may only involve the separation of TM1–TM2 pairs from TM3 (Fig. S3). It is also possible that the unstable open state in valine mutants has a different conformation compared with WT, which is predicted to have kink-free TM3 helices in the open state (Akitake et al., 2007).

The predicted inactivated state is susceptible to axial compaction coupled to lateral expansion of the TM domain The data above show that crowding acts synergistically with tension-driving inactivation. However, the question of how tension and crowding perturbations communicate within the channel remains. We designed steered simulations to mimic crowding pressure acting on the channel from the cytoplasmic side and observed a susceptibility of the resting and inactivated states to this type of perturbation. Although crowding pressure of smaller macromolecular components might be acting normally to the cage surface, larger crowders that are unable to approach the membrane too closely would primarily exert pressure along the main axis of the channel toward the membrane. In the following simulations, we have approximated the pressure acting on the cage domain in the direction normal to the membrane. The membrane-equilibrated models of the resting and inactivated state were subjected to gradually increasing steering force applied to all main chain atoms of the lower hemisphere of the cage directed toward the membrane midplane. The force increased exponentially from 0.001 to 0.1 kcal/mol/Å. These forces were purposely much larger than the actual osmotic forces acting on the cage in experiments to observe the character of domain interactions in the 20-ns time frame accessible in all-atom simulations. Fig. 7 (A and B) shows the initial and 16-ns frames of a 20-ns simulation of the resting (A) and inactivated models (B; after the 16th ns, the exponentially increasing force was causing nonphysiological distortion of the structures). Analysis of these two states indicates that the upward cage displacement resulted in sharpened TM3 kinks (at G113) and increased splay of TM1-TM2 pairs, stabilizing and somewhat exaggerating the inactivated state and causing a significant in-plane expansion. Steered motion of the cage in the resting model did not lead to such distortions and caused an increase in the in-plane channel area only half as large. Fig. 7 C shows the changes in the

molecule's geometry with time, tracing the distances between the cage and TM domain's centers of masses in the course of compression. Fig. 7 D depicts simultaneous changes of the volume that the cage takes in the cytoplasm and the mean in-plane area of the TM domain. It is clear that the vertical displacement of the cage, especially in the inactivated state, is coupled to a large lateral expansion of the TM domain. A volume change of  $\sim 20 \text{ nm}^3$  experienced by the cytoplasmic domain is substantial. Because the thermal energy of  $1 k_BT = 4.1$ atm  $\times$  1 nm<sup>3</sup>, the pressure that would generate this energy over a 20-nm<sup>3</sup> compression path is  $\sim$ 0.2 atm, which corresponds to an osmotic imbalance of only  $\sim$ 9 mOsM. Note that 10% wt/vol Ficoll 400 used in our experiments has an osmotic pressure of 70 mOsm, meaning that it creates an energy bias toward a more compact state by  $\sim$ 8 kT. A coupled expansion of the TM domain by  $\sim 8 \text{ nm}^2$  under tension of 7 mN/m would by itself generate a bias of  $\sim$ 14 kT toward the inactivated state. The observed coupling between the two geometrical parameters (Fig. 7, E and F) appears to be the structural underpinning of the enhancement of tension-driven inactivation by crowders.

Experiments presented on Fig. 3 A show that crowding agents also shift activation curves to the right, making opening harder. Based on simulations, crowding pressure could stabilize the resting conformation relative to the open one by making it slightly wider in the membrane and thus decreasing energy gain from tension on opening. Another stabilizing contribution might be increasing the number and stability of TM1-TM2 linker contacts with the β domains (in particular, the D62-R131 salt bridge). Such closed conformation would still be capable of opening because of the stable TM2-TM3 contact (membrane stress transmission route to the gate) but may open at a slightly higher tension, as observed in our experiments (Fig. 3 A, red traces). The inactivated state is predicted to be more strongly stabilized because of increased TM2-TM3 separation, which facilitates expansion of the TM1-TM2 barrel.

Consistent with the slow kinetics of inactivation (5-10 s at near-midpoint tensions), in our 20-ns steered simulation of the resting state, we did not observe any tendency to switch to the inactivated conformation even at highest axial pressures exerted on the cage. Neither did we observe recombination of the  $\beta$  domain with the TM3b helix. Apart from the timescale, it could be also because we did not apply high enough tension, which is required for triggering the transition as observed in our experiments in the absence or presence of Ficoll (Fig. 4, A and D). To visualize the transition, it would take a set of specially designed long simulations with simultaneously applied tension to the TM domain and pressure on the cage, and possibly enhanced sampling techniques, to overcome the energy barriers underlying the slow rate of inactivation.

#### DISCUSSION

The experimental measurements of MscS activity in excised patches using advanced pressure protocols (Fig. 2) show that the channel is exquisitely sensitive to crowding agents on the cytoplasmic side, which shift activation curves to higher tensions and drive immediate inactivation after the first activating pulse. Because resting MscS can undergo two parallel tension-driven transitions, to either the open or inactivated state, crowding appears to bias the process toward inactivation (Fig. S2). The volume percent of the crowders present in our experiments (5–10%) was lower than the typically estimated macromolecular excluded volume for *E. coli* cells grown under

standard conditions ( $\sim$ 30%; Zimmerman and Trach, 1991; Record et al., 1998). This means that the observed effect is not caused by exaggerated experimental conditions and thus pertains to the physiology of osmoregulation. How can this crowding-dependent MscS disengagement be beneficial for bacteria?

Solute-accessible volume of the cytoplasm (reciprocal to macromolecular excluded volume) is a parameter tightly regulated by cells through accumulation or release of small osmolytes. Bacterial mechanosensitive channels perceive excessive internal pressure in the form of membrane tension, which is generated in the cytoplasmic membrane in a curvature-dependent manner according

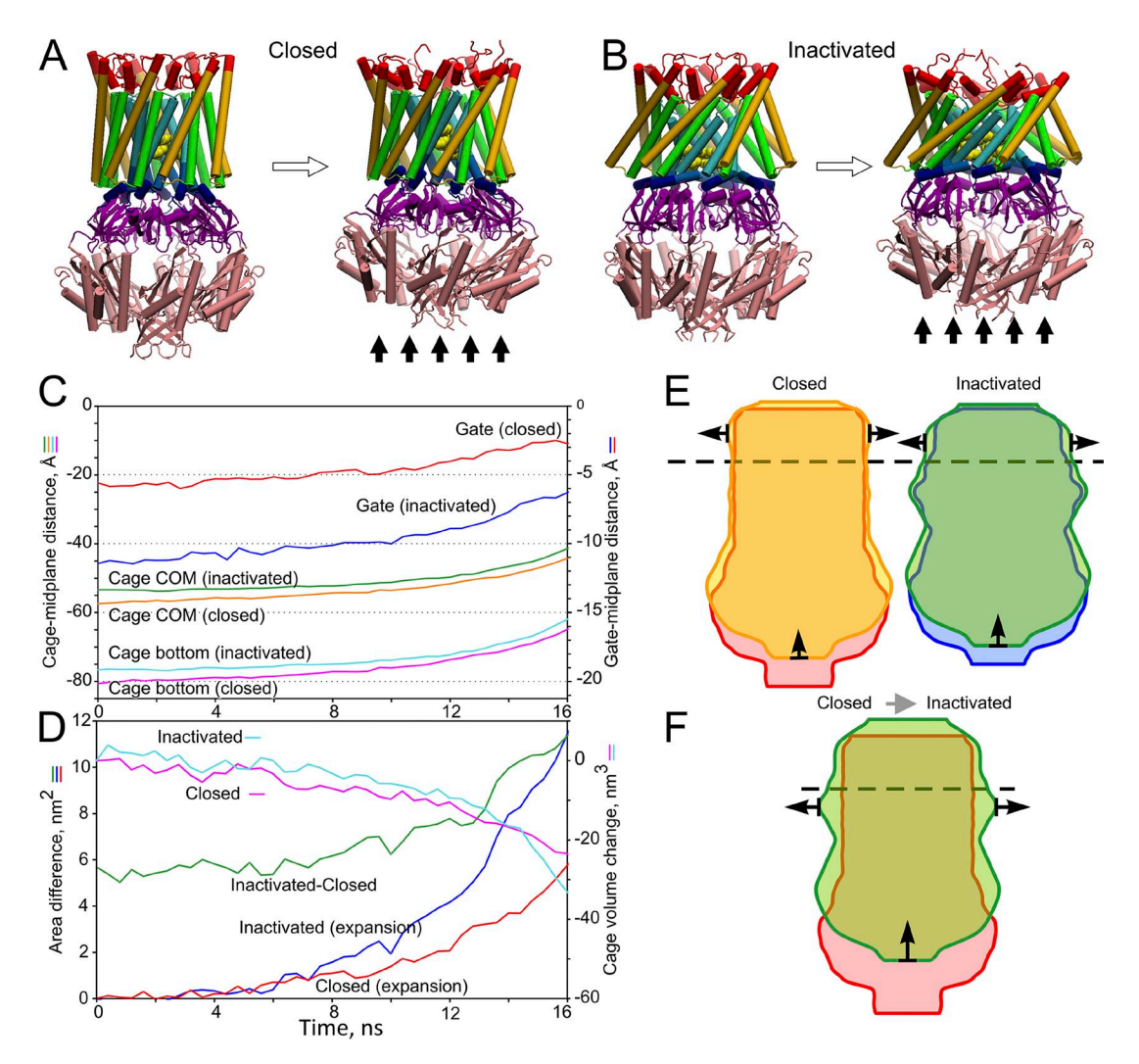


Figure 7. Results of MD simulations in which the cage domain in the resting and inactivated states was subjected to a compressive force applied to the lower half of the cage normally toward the plane of the membrane. (A and B) Closed and inactivate conformations at the start and at 8 ns (marked with black arrows). (C) The applied force causes similar displacement of the bottom and center of mass (COM) of the cage in both closed and inactivated states; however, the gate region displaces more toward the center of the membrane in the inactivated state (blue line), apparently because of the detached state of TM1–TM2 pairs from the TM3 barrel. (D) Cage volume decreases similarly under compression in both conformations; however, cage pressing on the TM barrel causes twice as large of an increase of the inplane area of the inactivated conformation as it has lipid-facing helices detached from the pore-lining TM3 barrel, thus favoring the transition from the closed to inactivated state under tension. (E and F) Cage compression and the barrel expansion are illustrated by the contours of cross section radii (E), whereas overlay of the closed state with no compression and inactivated state under force (F) explains the geometry change with inactivation and the reason for the synergy between tension and crowding pressure in driving inactivation.

to the law of Laplace. The cytoplasmic membrane of  $E.\ coli$  is not free but is instead covered by both an elastic peptidoglycan layer (cell wall; Koch and Woeste, 1992; Yao et al., 1999) and the outer membrane, which are stressed under normal turgor pressure of  $\sim$ 1–3.5 atm (Cayley et al., 2000) and undergo additional distension under osmotic downshock. We propose that the presence of an elastic cell wall acting as a corset stipulates a feedback system that would sense and modify the efflux of small osmolytes depending on the degree of cytoplasmic crowding.

Let us first consider a cell devoid of a cell wall that is initially in osmotic equilibrium with the external medium. On moderate medium dilution, hypoosmotic swelling will dilute internal osmolytes and reduce the osmotic gradient, but stronger swelling and building membrane tension will activate mechanosensitive channels, which would release part of the internal osmolytes and thus relieve the pressure inside. Once this tension drops to the subthreshold level, the channels close. As a result, this cell would gain some extra volume after the osmotic downshock, and this sequence cannot result in a return to previous levels of small solute accessible volume (illustrated in Fig. 8) unless the conditions suddenly reverse toward higher external osmolarity. Even if mechanosensitive channels remain open after establishing the new equilibrium in a more hypoosmotic medium, this would not result in a cell volume decrease.

MscS, which is attributed exclusively to walled cells (Pivetti et al., 2003; Balleza and Gómez-Lagunas, 2009), functions in a different context. Because of metabolite accumulation, bacterial cells typically have relatively high internal hydrostatic (turgor) pressure (Cayley et al., 2000). This pressure acting on the cytoplasmic membrane from the inside is counteracted by the compressing force from the cell wall, and this balance maintains cell volume and shape (Vollmer and Höltje, 2001).

Therefore, not only the internal volume but also the fraction occupied by macromolecules is the result of fine balance between the external compression and turgor created primarily by small metabolites. When in special experiments intracellular components were chemically washed away, the sacculus shrunk substantially (Yao et al., 1999). A qualitatively similar effect is expected in the event of osmotic membrane permeabilization. When mechanosensitive channels are open under osmotic downshock, the release of osmolytes and simultaneous water efflux are greatly assisted by the elastic recoil of the peptidoglycan. A prolonged action of channels in this case can potentially let out more osmolytes than needed, resulting in excessive condensation of the cytoplasm. A feedback system that would detect excessive crowding and timely disengage the channels will prevent cell shrinkage and cytoplasm "over-draining." The behavior of MscS in the presence of crowders described above clearly indicates the presence of such a feedback.

Our data show that the crowding-sensing mechanism increases the rate of tension-driven inactivation, which involves the hollow cytoplasmic domain (cage). Searches for conformations that satisfy the presence of functionally important D62-R128/R131 salt bridges (Nomura et al., 2008) resulted in a new arrangement of helices in the TM domain, which straightened the G113 crystallographic kink and led to the separation of the TM3b segment from the  $\beta$  domains in the cage. This conformation characterized by tight interactions between the peripheral (TM1-TM2) helices and the gate region (TM3) was assigned as the resting state, whereas the splayed crystal-like model was considered inactivated. The detachment of the B domain from TM3b resulted in a slightly more prolate conformation of the cage as compared with the inactivated state with β domains attached to TM3b (Fig. 1, A and B). Subjected to steered compression in MD simulations (Fig. 7), the two conformations

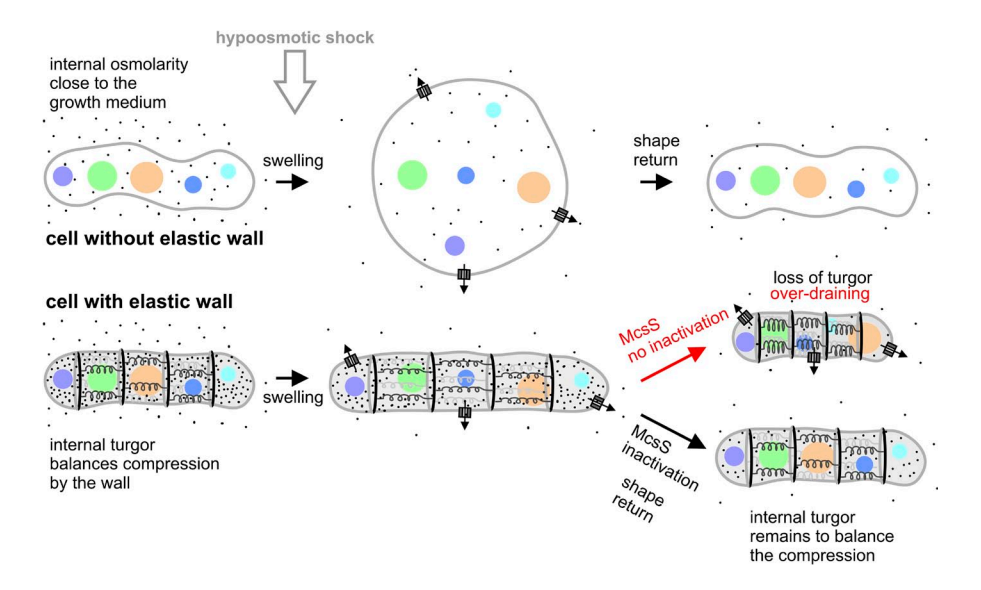


Figure 8. A cartoon representation of wall-less and walled cell responses to osmotic downshifts. The wall-less cell (top) behaves like an osmometer with release valves: it swells first and opens osmolyte release channels and partially returns to its initial state, which is close to equilibrium with the new more dilute medium. Shrinkage is not expected. The walled cell maintains its volume by generating turgor pressure that counters the restoring force of the elastic cell wall. Swelling and opening of mechanosensitive channels will release osmolytes and water, but if the channels remain open for too long, the compression may extrude water and shrink the cell beyond its normal volume. Channels that sense the increasing cytoplasmic crowding will inactivate and prevent over-draining of the cytoplasm.

exhibited similar compliances in the axial direction but very different lateral expansions of the TM domain. These suggested that when the closed channel experiences tension and starts switching from the resting to the inactivated state (Kamaraju et al., 2011), not only does it expand in the plane of the membrane, but it also becomes more receptive to crowding forces acting on the cage. The simulations strongly suggest an allosteric interplay between the geometries of the TM and cytoplasmic domains that makes the bulk parameter of macromolecular pressure inside the cell act synergistically with the interfacial parameter of membrane tension.

How does this coupling occur? Our data suggest that crowding pressure by itself (in the studied range) does not produce inactivation, but moderate tension applied to the peripheral TM helices is required to trigger the transition. Under super-threshold tension and low/no crowding pressure the channel willingly activates. When crowding increases, the resting state is stabilized and the activation threshold increases. However, when this threshold is reached, tension diverts the population into the inactivation path (Fig. 2 and Fig. S4). We have pinpointed several loci in the channel that change in the course of the inactivating transition. The major event is kink formation at G113 (Akitake et al., 2007), which accompanies detachment of the TM1-TM2 pairs from the gate and produces lateral splay, which in turn increases the "footprint" of the channel inside the membrane (Kamaraju et al., 2011). The G113-kinked conformation of TM3s is then critically stabilized by association with the  $\beta$  domains in the cage. This last step is supported by the effect of contact-destabilizing mutation G168D (Fig. 4), the mutant which barely inactivates and is practically insensitive to crowder-induced inactivation. Importantly, G168D MscS does not inactivate with strong depolarizing voltage either (Fig. 5), indicating that voltage-driven inactivation (Vasquez and Perozo, 2004; Akitake et al., 2005) proceeds through the same pathway as the crowder-assisted inactivation. According to the inflected traces in Fig. 5, it may not be voltage per se, but more likely ionic current and an associated electroosmotic efflux of water (Anishkin et al., 2008b) that tends to reduce the internal volume of the cage and collapse TM3s, which might be analogous to the effect of crowders. Previous studies (Akitake et al., 2007; Belyy et al., 2010b) have shown that this buckling of TM3 at G113 (and thus inactivation) can be inhibited via a G113A substitution, which increases the helical propensity at that point. The fact that G113A is more susceptible than G168D to crowder-induced inactivation indicates that the association of TM3 and the  $\beta$  domain is not just a major requirement of inactivation but can impose a kink in TM3 even in the presence of G113A.

In steered simulations under normal force mimicking the effect of crowding pressure, we observed a clear difference in the behavior of the modeled resting and inactivated states. In the latter case, the detachment of the TM1–TM2 pairs from TM3s and lateral barrel expansion is reinforced by the normal pressure. Thus, under conditions where both a normal force (crowding) and membrane tension are applied, the inactivated state of the channel is favored.

The effects of mutations stabilizing the TM3b-β association (N117V and N167V) were more complex. These mutations strongly destabilized the open state even at saturating tensions, leading to speedy inactivation in the absence of crowders. The recovery of these mutants from the inactivated state was unexpectedly fast (Fig. 6), suggesting that the closed and inactivated states in these mutants are more similar than in the WT and the conformational path for recovery is shorter. The modeling predicted that even with the stable G113 kink imposed by stable association of TM3b with the β domain, the TM1-TM2 loops can salt-bridge to the equatorial arginines (R128 or R131) and the helices themselves can form buried contact with the gate such that the channel can open, although at tensions higher than normal (Fig. S3). The effectively shorter pathway between the closed and inactivated states in these mutants is likely caused by the absence of the vertical TM3 barrel displacement impeded by the stabilized G113 kinks.

In conclusion, the fraction of cell volume allocated for macromolecules is a parameter tightly regulated by cells through accumulation or release of small osmolytes. We have only begun to understand mechanisms that regulate the crowding-dependent transport of osmolytes across the membrane. In the present work we show that MscS, the primary turgor-regulating valve in E. coli, is also one of the sensors of internal crowding. Following the earlier observations by Grajkowski et al. (2005) and Koprowski et al. (2007, 2011), we have characterized MscS as the first sensor of cytoplasmic crowding and explained its adaptive inactivation mechanism in the context of a small cell encased in an elastic peptidoglycan sacculus. Although not all MscS homologues found in other species inactivate (Nakayama et al., 2013; Petrov et al., 2013), this mechanism has implications for the entire family of MscS-like channels carrying similar cytoplasmic cages that are structurally connected to the gate through the pore-lining helices. This domain, previously considered as a prefilter (Naismith and Booth, 2012), was recently shown to impart some ionic selectivity to MscS and its homologues (Zhang et al., 2012; Cox et al., 2013). Our data now provide the first conjecture as to why MscS-like channels are ubiquitously distributed in all domains of life characterized by cell walls and a reliance on turgor for the maintenance of their volume, shape, and mechanical strength.

We thank Dr. Miriam Boer and Mrs. Abigail Cember for assistance with cloning, mutagenesis, and primary characterization of some mutants.

This work was supported by National Institutes of Health grants GM075225 and GM107652 to S. Sukharev.

The authors declare no competing financial interests.

Sharona E. Gordon served as editor.

Submitted: 28 September 2013 Accepted: 2 April 2014

### REFERENCES

- Akitake, B., A. Anishkin, and S. Sukharev. 2005. The "dashpot" mechanism of stretch-dependent gating in MscS. J. Gen. Physiol. 125:143–154. http://dx.doi.org/10.1085/jgp.200409198
- Akitake, B., A. Anishkin, N. Liu, and S. Sukharev. 2007. Straightening and sequential buckling of the pore-lining helices define the gating cycle of MscS. *Nat. Struct. Mol. Biol.* 14:1141–1149. http://dx .doi.org/10.1038/nsmb1341
- Anishkin, A., B. Akitake, and S. Sukharev. 2008a. Characterization of the resting MscS: modeling and analysis of the closed bacterial mechanosensitive channel of small conductance. *Biophys. J.* 94:1252–1266. http://dx.doi.org/10.1529/biophysj.107.110171
- Anishkin, A., K. Kamaraju, and S. Sukharev. 2008b. Mechanosensitive channel MscS in the open state: modeling of the transition, explicit simulations, and experimental measurements of conductance. *J. Gen. Physiol.* 132:67–83. http://dx.doi.org/10.1085/jgp.200810000
- Anishkin, A., A.L. Milac, and H.R. Guy. 2010. Symmetry-restrained molecular dynamics simulations improve homology models of potassium channels. *Proteins*. 78:932–949. http://dx.doi.org/10.1002/prot.22618
- Balleza, D., and F. Gómez-Lagunas. 2009. Conserved motifs in mechanosensitive channels MscL and MscS. Eur. Biophys. J. 38:1013–1027. http://dx.doi.org/10.1007/s00249-009-0460-y
- Bass, R.B., P. Strop, M. Barclay, and D.C. Rees. 2002. Crystal structure of *Escherichia coli* MscS, a voltage-modulated and mechanosensitive channel. *Science*. 298:1582–1587. http://dx.doi.org/10.1126/ science.1077945
- Belyy, V., A. Anishkin, K. Kamaraju, N. Liu, and S. Sukharev. 2010a. The tension-transmitting 'clutch' in the mechanosensitive channel MscS. *Nat. Struct. Mol. Biol.* 17:451–458. http://dx.doi.org/10.1038/nsmb.1775
- Belyy, V., K. Kamaraju, B. Akitake, A. Anishkin, and S. Sukharev. 2010b. Adaptive behavior of bacterial mechanosensitive channels is coupled to membrane mechanics. *J. Gen. Physiol.* 135:641–652. http://dx.doi.org/10.1085/jgp.200910371
- Boer, M., A. Anishkin, and S. Sukharev. 2011. Adaptive MscS gating in the osmotic permeability response in *E. coli*: the question of time. *Biochemistry*. 50:4087–4096. http://dx.doi.org/10.1021/bi1019435
- Cayley, S., and M.T. Record Jr. 2003. Roles of cytoplasmic osmolytes, water, and crowding in the response of *Escherichia coli* to osmotic stress: biophysical basis of osmoprotection by glycine betaine. *Biochemistry*. 42:12596–12609. http://dx.doi.org/10.1021/bi0347297
- Cayley, S., B.A. Lewis, H.J. Guttman, and M.T. Record Jr. 1991. Characterization of the cytoplasm of *Escherichia coli* K-12 as a function of external osmolarity: Implications for protein-DNA interactions in vivo. *J. Mol. Biol.* 222:281–300. http://dx.doi.org/10.1016/0022-2836(91)90212-O
- Cayley, D.S., H.J. Guttman, and M.T. Record Jr. 2000. Biophysical characterization of changes in amounts and activity of *Escherichia coli* cell and compartment water and turgor pressure in response to osmotic stress. *Biophys. J.* 78:1748–1764. http://dx.doi.org/10.1016/S0006-3495(00)76726-9
- Cox, C.D., T. Nomura, C.S. Ziegler, A.K. Campbell, K.T. Wann, and B. Martinac. 2013. Selectivity mechanism of the mechanosensitive

- channel MscS revealed by probing channel subconducting states. *Nat. Commun.* 4:2137. http://dx.doi.org/10.1038/ncomms3137
- Csonka, L.N., and A.D. Hanson. 1991. Prokaryotic osmoregulation: genetics and physiology. *Annu. Rev. Microbiol.* 45:569–606. http://dx.doi.org/10.1146/annurev.mi.45.100191.003033
- Edwards, M.D., S. Black, T. Rasmussen, A. Rasmussen, N.R. Stokes, T.L. Stephen, S. Miller, and I.R. Booth. 2012. Characterization of three novel mechanosensitive channel activities in *Escherichia coli. Channels* (Austin). 6:272–281. http://dx.doi.org/10.4161/chan.20998
- Ellis, R.J. 2001. Macromolecular crowding: an important but neglected aspect of the intracellular environment. *Curr. Opin. Struct. Biol.* 11:114–119. http://dx.doi.org/10.1016/S0959-440X(00)00172-X
- Grajkowski, W., A. Kubalski, and P. Koprowski. 2005. Surface changes of the mechanosensitive channel MscS upon its activation, inactivation, and closing. *Biophys. J.* 88:3050–3059. http://dx.doi.org/10.1529/biophysj.104.053546
- Humphrey, W., A. Dalke, and K. Schulten. 1996. VMD: visual molecular dynamics. J. Mol. Graph. 14:33–38. http://dx.doi.org/10.1016/0263-7855(96)00018-5
- Kamaraju, K., V. Belyy, I. Rowe, A. Anishkin, and S. Sukharev. 2011. The pathway and spatial scale for MscS inactivation. *J. Gen. Physiol.* 138:49–57. http://dx.doi.org/10.1085/jgp.201110606
- Koch, A.L., and S. Woeste. 1992. Elasticity of the sacculus of Escherichia coli. J. Bacteriol. 174:4811–4819.
- Koprowski, P., W. Grajkowski, and A. Kubalski. 2007. The MscS cytoplasmic domain and its conformational changes on the channel gating. In *Mechanosensitive Ion Channels, Part 1*. Current Topics in Membranes, Vol. 58. O.P. Hamill, editor. Academic Press, San Diego. 295–309.
- Koprowski, P., W. Grajkowski, E.Y. Isacoff, and A. Kubalski. 2011. Genetic screen for potassium leaky small mechanosensitive channels (MscS) in *Escherichia coli*: recognition of cytoplasmic β domain as a new gating element. *J. Biol. Chem.* 286:877–888. http://dx.doi.org/10.1074/jbc.M110.176131
- Lai, J.Y., Y.S. Poon, J.T. Kaiser, and D.C. Rees. 2013. Open and shut: crystal structures of the dodecylmaltoside solubilized mechanosensitive channel of small conductance from *Escherichia coli* and *Helicobacter pylori* at 4.4 Å and 4.1 Å resolutions. *Protein Sci.* 22:502–509. http://dx.doi.org/10.1002/pro.2222
- Levina, N., S. Tötemeyer, N.R. Stokes, P. Louis, M.A. Jones, and I.R. Booth. 1999. Protection of *Escherichia coli* cells against extreme turgor by activation of MscS and MscL mechanosensitive channels: identification of genes required for MscS activity. *EMBO J.* 18:1730–1737. http://dx.doi.org/10.1093/emboj/18.7.1730
- Li, Y., P.C. Moe, S. Chandrasekaran, I.R. Booth, and P. Blount. 2002. Ionic regulation of MscK, a mechanosensitive channel from *Escherichia coli. EMBO J.* 21:5323–5330. http://dx.doi.org/10.1093/emboj/cdf537
- Liedtke, W. 2005. TRPV4 as osmosensor: a transgenic approach. Pflugers Arch. 451:176–180. http://dx.doi.org/10.1007/s00424-005-1449-8
- Machiyama, H., H. Tatsumi, and M. Sokabe. 2009. Structural changes in the cytoplasmic domain of the mechanosensitive channel MscS during opening. *Biophys. J.* 97:1048–1057. http://dx.doi.org/10.1016/j.bpj.2009.05.021
- Martinac, B., M. Buechner, A.H. Delcour, J. Adler, and C. Kung. 1987.
  Pressure-sensitive ion channel in *Escherichia coli. Proc. Natl. Acad. Sci. USA*. 84:2297–2301. http://dx.doi.org/10.1073/pnas.84.8.2297
- Minton, A.P. 1998. Molecular crowding: analysis of effects of high concentrations of inert cosolutes on biochemical equilibria and rates in terms of volume exclusion. *Methods Enzymol.* 295:127–149. http://dx.doi.org/10.1016/S0076-6879(98)95038-8
- Naismith, J.H., and I.R. Booth. 2012. Bacterial mechanosensitive channels—MscS: evolution's solution to creating sensitivity in function. *Annu. Rev. Biophys.* 41:157–177. http://dx.doi.org/10.1146/annurev-biophys-101211-113227

- Nakayama, Y., K. Yoshimura, and H. Iida. 2013. Electrophysiological characterization of the mechanosensitive channel MscCG in *Corynebacteriumglutamicum.Biophys. J.* 105:1366–1375.http://dx.doi.org/10.1016/j.bpj.2013.06.054
- Nomura, T., M. Sokabe, and K. Yoshimura. 2008. Interaction between the cytoplasmic and transmembrane domains of the mechanosensitive channel MscS. *Biophys. J.* 94:1638–1645. http://dx.doi.org/10.1529/biophysj.107.114785
- Petrov, E., D. Palanivelu, M. Constantine, P.R. Rohde, C.D. Cox, T. Nomura, D.L. Minor Jr., and B. Martinac. 2013. Patch-clamp characterization of the MscS-like mechanosensitive channel from *Silicibacter pomeroyi*. *Biophys. J.* 104:1426–1434. http://dx.doi.org/10 .1016/j.bpj.2013.01.055
- Pivetti, C.D., M.R. Yen, S. Miller, W. Busch, Y.H. Tseng, I.R. Booth, and M.H. Saier Jr. 2003. Two families of mechanosensitive channel proteins. *Microbiol. Mol. Biol. Rev.* 67:66–85. http://dx.doi.org/ 10.1128/MMBR.67.1.66-85.2003
- Record, M.T. Jr., E.S. Courtenay, S. Cayley, and H.J. Guttman. 1998. Biophysical compensation mechanisms buffering *E. coli* protein-nucleic acid interactions against changing environments. *Trends Biochem. Sci.* 23:190–194. http://dx.doi.org/10.1016/S0968-0004(98)01207-9
- Reiser, V., D.C. Raitt, and H. Saito. 2003. Yeast osmosensor Sln1 and plant cytokinin receptor Cre1 respond to changes in turgor pressure. *J. Cell Biol.* 161:1035–1040. http://dx.doi.org/10.1083/jcb.200301099
- Schumann, U., M.D. Edwards, T. Rasmussen, W. Bartlett, P. van West, and I.R. Booth. 2010. YbdG in *Escherichia coli* is a thresholdsetting mechanosensitive channel with MscM activity. *Proc. Natl. Acad. Sci. USA*. 107:12664–12669. http://dx.doi.org/10.1073/pnas .1001405107
- Sotomayor, M., and K. Schulten. 2004. Molecular dynamics study of gating in the mechanosensitive channel of small conductance MscS. *Biophys. J.* 87:3050–3065. http://dx.doi.org/10.1529/biophysj
- Steinbacher, S., R. Bass, P. Strop, and D.C. Rees. 2007. Structures of the prokaryotic mechanosensitive channels MscL and MscS. In Mechanosensitive Ion Channels, Part 1. Current Topics in Membranes, Vol. 58. O.P. Hamill, editor. Academic Press, San Diego. 1–24.
- Sukharev, S.I., P. Blount, B. Martinac, F.R. Blattner, and C. Kung. 1994. A large-conductance mechanosensitive channel in *E. coli* encoded by mscL alone. *Nature.* 368:265–268. http://dx.doi.org/10.1038/368265a0
- Sukharev, S.I., W.J. Sigurdson, C. Kung, and F. Sachs. 1999. Energetic and spatial parameters for gating of the bacterial large conductance mechanosensitive channel, MscL. J. Gen. Physiol. 113:525–540. http://dx.doi.org/10.1085/jgp.113.4.525
- Sukharev, S., B. Akitake, and A. Anishkin. 2007. The bacterial mechanosensitive channel MscS: Emerging principles of gating and modulation. In *Mechanosensitive Ion Channels, Part 1*. Current Topics in Membranes, Vol. 58. O.P. Hamill, editor. Academic Press, San Diego. 235–267.

- van den Berg, B., R.J. Ellis, and C.M. Dobson. 1999. Effects of macromolecular crowding on protein folding and aggregation. EMBO J. 18:6927–6933. http://dx.doi.org/10.1093/emboj/18.24
- Vasquez, V., and E. Perozo. 2004. Voltage dependent gating in MscS. *Biophys. J.* 86:545A.
- Vásquez, V., M. Sotomayor, D.M. Cortes, B. Roux, K. Schulten, and E. Perozo. 2008. Three-dimensional architecture of membrane-embedded MscS in the closed conformation. *J. Mol. Biol.* 378: 55–70. http://dx.doi.org/10.1016/j.jmb.2007.10.086
- Vollmer, W., and J.V. Höltje. 2001. Morphogenesis of *Escherichia coli. Curr. Opin. Microbiol.* 4:625–633. http://dx.doi.org/10.1016/S1369-5274(01)00261-2
- Wang, L.C., L.K. Morgan, P. Godakumbura, L.J. Kenney, and G.S. Anand. 2012. The inner membrane histidine kinase EnvZ senses osmolality via helix-coil transitions in the cytoplasm. *EMBO J.* 31:2648–2659. http://dx.doi.org/10.1038/emboj.2012.99
- Wang, W., S.S. Black, M.D. Edwards, S. Miller, E.L. Morrison, W. Bartlett, C. Dong, J.H. Naismith, and I.R. Booth. 2008. The structure of an open form of an *E. coli* mechanosensitive channel at 3.45 Å resolution. *Science*. 321:1179–1183. http://dx.doi.org/10.1126/science.1159262
- Wood, J.M. 1999. Osmosensing by bacteria: signals and membranebased sensors. *Microbiol. Mol. Biol. Rev.* 63:230–262.
- Wood, J.M. 2007. Bacterial osmosensing transporters. *Methods Enzymol*. 428:77–107. http://dx.doi.org/10.1016/S0076-6879(07) 28005-X
- Wood, J.M., E. Bremer, L.N. Csonka, R. Kraemer, B. Poolman, T. van der Heide, and L.T. Smith. 2001. Osmosensing and osmoregulatory compatible solute accumulation by bacteria. *Comp. Biochem. Physiol. A Mol. Integr. Physiol.* 130:437–460. http://dx.doi.org/ 10.1016/S1095-6433(01)00442-1
- Yao, X., M. Jericho, D. Pink, and T. Beveridge. 1999. Thickness and elasticity of gram-negative murein sacculi measured by atomic force microscopy. *J. Bacteriol.* 181:6865–6875.
- Yoshimura, K., A. Batiza, and C. Kung. 2001. Chemically charging the pore constriction opens the mechanosensitive channel MscL. *Biophys. J.* 80:2198–2206. http://dx.doi.org/10.1016/S0006-3495 (01)76192-9
- Zhang, X., J. Wang, Y. Feng, J. Ge, W. Li, W. Sun, I. Iscla, J. Yu, P. Blount, Y. Li, and M. Yang. 2012. Structure and molecular mechanism of an anion-selective mechanosensitive channel of small conductance. *Proc. Natl. Acad. Sci. USA*. 109:18180–18185. http://dx.doi.org/10.1073/pnas.1207977109
- Zhou, H.X., G. Rivas, and A.P. Minton. 2008. Macromolecular crowding and confinement: biochemical, biophysical, and potential physiological consequences. *Annu. Rev. Biophys.* 37:375–397. http://dx.doi.org/10.1146/annurev.biophys.37.032807.125817
- Zimmerman, S.B., and S.O. Trach. 1991. Estimation of macromolecule concentrations and excluded volume effects for the cytoplasm of *Escherichia coli. J. Mol. Biol.* 222:599–620. http://dx.doi.org/10.1016/0022-2836(91)90499-V